CHAPTER 4 THREE-DIMENSIONAL ANALYSIS -- NUMERICAL MODEL A

4.1 INTRODUCTION

This chapter describes the three-dimensional analysis of a single pipe. This single pipe model is used to obtain information about the overall behaviour of the concrete pipe under different loading conditions and to carry out back analysis of Ripley's (1989) experimental data from small-scale model pipes. The more detailed models, involving a pipe with its surrounding soil and a symmetric three-pipe system, are discussed in Chapters 5 and 6 respectively. The pipe was treated as a three-dimensional structure because the applied load was non-uniformly distributed at the pipe end due to the misalignment of the pipeline in practice. Moreover, since the pipe is a regular structure in a cylindrical co-ordinate system, the advantage of this system has been taken to simplify the input data and to make the output results more readable.

In this chapter, the single pipe model is described in Section 4.2. The effect of load distribution and the effect of the pipe wall thickness are discussed in Sections 4.3 and 4.4 respectively. The conclusion from this model is given in Section 4.5. Finally, a numerical back analysis of Ripley's (1989) experimental data is discussed in Section 4.6.

4.2 NUMERICAL MODEL A

The numerical model A, a single concrete pipe, and its finite element mesh are shown in Figure 4.1 (since the geometry of the pipe and the applied loads are symmetrical about the plane of $y = 0$, just half of the pipe was used in the analysis as shown in the figure). The pipe

is shown in Figure 4.1(a); a surface of r = constant unfolded on a plane is shown in Figure 4.1(b); the top end of the pipe in Figure 4.1(c) and the section $\theta = 0^0$ in Figure 4.1(d). The element type used in the analysis was 8-node hexahedron. The pipe was treated as linearly elastic and the material constants obtained by Ripley (1989), the Young's modulus E_c = 31700MPa and the Poisson's ratio μ_c = 0.2, were used in the analysis for the convenience of comparison between the numerical results and Ripley's experimental data. The dimensions of the pipe are the same as those of the test pipes used by Ripley in his experiment and are shown in Figure 4.1(d). To investigate the effect of the thickness of the pipe wall, both the thick wall (wall thickness t = 25mm) and the thin wall (t = 14.3mm) pipe were included in the analysis.

4.3 EFFECT OF LOAD DISTRIBUTION

In this section, the effect of the load distribution is examined using the thick wall pipe. The analysis was carried out with two different types of applied loads, the 'edge' loading and the 'diagonal' loading. These two types of loading are the extreme loading condition of pipes in practice due to the misalignment of the pipe line.

4.3.1 EDGE LOADING WITH THICK WALL PIPE

The first analysis is with the 'edge' loading which is transferred along one edge of the pipe. The total load applied in the analysis was P = 5kN. To study the effect of different load distributions, the analysis included three types of 'edge' loading: the bi-linearly distributed concentrated load (case E1), the uniform load on the outer half thickness of the pipe end over 22 degrees in the circumferential direction (case E2) and the uniform load across the pipe thickness over 11 degrees in the circumferential direction (case E3). All three load

distributions on the upper pipe end are shown in Figure 4.2 and the load distributions on the bottom pipe end are the same as those on the upper end except in the opposite direction. All the loading conditions are simplified approximations to extreme conditions in practice. In the numerical analysis, in addition to the symmetrical condition on the plane of $y = 0$ (that is, all the nodes on that plane were fixed in the y direction), three nodes on the external surface at each end of the pipe at the loaded edge were fixed in the x direction and the node at the bottom loaded corner was fixed in the z direction as well as shown in Figure 4.3(a) and 4.3(c).

If the load (P = 5kN) is uniformly distributed over the pipe end (half of the pipe in the analysis), the average pressure over the pipe end is q = 0.73MPa. For convenience of result comparison, all the computed stresses in the thick wall pipe in this chapter are normalised by this pressure when presented in the stress contours.

The results of the normalized most tensile principal stresses in the thick pipe under the 'edge' load are shown in Figure 4.4. The result for the case E1 is in Figure 4.4(a), the case E2 in Figure 4.4(b) and the case E3 in Figure 4.4(c). From the figure, it is clear that in all three cases the stresses are concentrated in two small regions which are adjacent to the loaded areas on the two pipe ends, while the stresses in other regions are very small except that some tensile stresses exist at the middle length of the pipe in the region of $\theta = 180^0$ on the internal surface. The highest stress is in the case E1 and the maximum value of stress in the load case E3 is the smallest of the three. The stresses are symmetrical about the middle section of the pipe in the z direction (that is, the section of z = 116mm) since the loads are symmetric about this plane. The direction of the most tensile principal stress within the pipe is complex and difficult to be expressed in a three-dimensional contour. However, in the two high tensile stress regions on the internal surface, the tensile stresses are mainly in hoop direction in all three loading cases as shown in Figure 4.4(d).

The normalized most compressive principal stresses in the thick pipe under the 'edge' load are shown in Figure 4.5. The results of the case E1, E2 and E3 are shown in Figure 4.5(a), 4.5(b) and 4.5(c) respectively. The figure clearly shows that the stresses are concentrated at the two loaded corners, while the stresses in other regions are very small; and that on the pipe ends the distribution patterns of the stresses are similar to those of the loads. Again, the highest magnitude of the stress is in the case E1, and the peak magnitudes of stress in case E2 and E3 are similar.

4.3.2 DIAGONAL LOADING WITH THICK WALL PIPE

The 'diagonal' loading is another type of extreme loading condition in practice. Under the 'diagonal' loading condition, the load is transferred diagonally between the opposite corners of the concrete pipe. Again three types of 'diagonal' loading were included in the analysis: the bi-linearly distributed concentrated load (case D1), the uniform load on the outer half thickness of the pipe end over 22 degrees in the circumferential direction (case D2) and the uniform load across the pipe thickness over 11 degrees in the circumferential direction (case D3). The total applied load was also P = 5kN as under the 'edge' loading condition. On the upper end of the pipe, the load distribution for each load was the same as that of the corresponding 'edge' load as shown in Figure 4.2. However, on the bottom end of the pipe, the load distribution of each load was obtained by rotating the corresponding 'edge' load through 180 degrees in the θ direction (that is, the load was in the region of $\theta = 0^0$ at the bottom end of the pipe). For the boundary condition, three nodes between $\theta = 169^0$ and $\theta = 180^0$ on the external surface at the upper end of the pipe were fixed in the x direction, as were the three nodes between $\theta = 0^0$ and $\theta = 11^0$ on the external surface at the bottom end of the pipe as shown in Figure 4.3(b) and 4.3(d). The symmetrical condition on the plane $y = 0$ was also applied.

From Figure 4.3(b), it is clear that under 'diagonal' loading condition, the constraints have to produce reaction forces to prevent rotation of the pipe, and these reaction forces are dependent on the type and the location of the constraints. This means that the computed stresses may be affected by the local effect of the constraints. The boundary conditions used in this chapter may represent a boundary condition in which the pipe is surrounded by hard rocks or a constraint condition used in laboratory tests, which might deviate from the boundary condition in practice. However, this effect of local constraints will be overcome by including the surrounding soil in the analysis in Chapter 5.

The normalized most tensile principal stresses in the thick wall pipe under the 'diagonal' loading are shown in Figure 4.6, with the result of the load case D1, D2 and D3 in Figure 4.6(a), 4.6(b) and 4.6(c) respectively. From the figure, it is clear that the in all cases high stresses appear in the two regions near the two loaded diagonal corners on the internal surface of the pipe, and that the stresses are almost zero in the region of $\theta = 90^0$ and are small at the other two diagonal corners. The peak values of the stress are higher than those under 'edge' loading condition, but the differences between the three cases are less than for the 'edge' loading. The highest tensile stress is in the case D1. Again, the distribution of the directions of the principal stresses are complex. However, on the internal surface of the pipe the directions of the principal stresses in the small regions with high tensile stresses are somewhat similar in all three cases and are approximately shown in Figure 4.6(d). In general, the principal tensile stresses in the region of $\theta = 180^0$ and 0^0 are mainly in the hoop direction, and when away towards to the central region of $\theta = 90^0$ the direction of the principal tensile stress changes from the hoop direction towards to the direction normal to the line connecting the two loaded corners.

To view the stresses on the external surface of the pipe, the pipe has been rotated through 180 degrees in the θ direction and the same most tensile principal stresses are now shown in Figure 4.7. Clearly, the stress distributions on the external surface are different

from those on the internal surface of the pipe. On the external surface of the pipe, the high stresses are located in the region of $\theta = 90^0$, however, the peak values are much lower than those on the internal surface. The stresses in other regions are very small (the high stress points near the loaded diagonal corner are possibly caused by the effect of local constraint as discussed above in this section and is examined in Chapter 5). The directions of the principal stresses in the region $\theta = 90^0$ are similar in all three cases and shown in Figure 4.7(d). The figure shows that the tensile direction changes from the hoop direction at two pipe ends to the direction normal to the line connecting the two loaded corners at the central area on the surface.

The normalized most compressive principal stresses in the thick wall pipe under 'diagonal' loading D1, D2 and D3 are shown in Figure 4.8(a), 4.8(b) and 4.8(c) respectively. Again the figure clearly shows that the stresses are highly concentrated in the two diagonal loaded corners. The low stresses are located in the band connecting the two loaded corners. And the stress patterns and the peak magnitudes of the stress are similar in all three cases.

4.4 EFFECT OF THE THICKNESS OF THE PIPE WALL

The analysis of the effect of the pipe wall thickness was carried out using the thin wall pipe under similar loading conditions as described in Section 4.3. The results are compared with those in the thick wall pipe in Section 4.3.

4.4.1 EDGE LOADING WITH THIN WALL PIPE

The finite element mesh and the boundary conditions were the same as those described in the last section as shown in Figure 4.1 and 4.3, except that the thickness of the pipe wall was 14.3mm instead of 25.0mm. The total applied load was also P = 5kN. The three 'edge'

loads (EN1, EN2 and EN3) have the same distribution patterns on the pipe ends as those in case E1, E2 and E3 in Section 4.3 as shown in Figure 4.2 except that the load intensity is higher than in Section 4.3 due to the reduced pipe wall thickness. Now the average pressure is q = 1.20MPa when the applied load is uniformly distributed over the end of the thin wall pipe. The computed stresses in the thin wall pipe have been normalised with respect to this pressure in all the stress contours in this chapter.

The normalized most tensile principal stresses in the thin wall pipe under 'edge' loading are shown in Figure 4.9(a), 4.9(b) and 4.9(c) for the loading case EN1, EN2 and EN3 respectively. As expected, the figure shows that the stress distribution patterns are similar to those in the thick wall pipe for all three loading cases except that the peak values of the normalised stress are slightly higher. Again the highest stress is in the case EN1. The most tensile principal stresses in the high stress regions are mainly in the hoop direction in all three cases as in the thick wall pipe (refer to section 4.3.1 and see Figure 4.4(d)). As for the normalized most compressive principal stresses in the thin wall pipe, the stress patterns and the peak magnitudes of the normalized stress in all three cases are similar to those in the thick wall pipe and are not discussed in detail here (refer to the Section 4.3.1 and see Figure 4.5).

4.4.2 DIAGONAL LOADING WITH THIN WALL PIPE

Similarly, under the 'diagonal' loading condition, the finite element mesh, the boundary conditions and the total applied load were the same as those in the analysis with the thick wall pipe. The only parameter changed was the thickness of the pipe wall. The three 'diagonal' loads called DN1, DN2 and DN3 have the same distributions on the two pipe ends as those of D1, D2 and D3 in section 4.3.2 as shown in Figure 4.2 except with higher load intensity due to the reduction of the wall thickness of the pipe as discussed under the 'edge' loading condition.

The results of the normalized most tensile principal stresses in the thin wall pipe under the three 'diagonal' loads are shown in Figure 4.10(a), 4.10(b) and 4.10(c) respectively. The figure shows that in all three cases the stress distribution patterns are similar to those in the thick wall pipe, however the peak values of the normalised stress are higher than those in the thick wall pipe. The regions of the high stresses now extend further towards the non-loaded corners of the concrete pipe along the z direction. The distribution patterns of the principal direction in the high stress regions on the internal pipe surface are similar in all three cases as shown in Figure 4.10(d). On the external surface of the pipe, the high stresses are located in the region of $\theta = 90^0$ as in the thick wall pipe except that the stresses are higher than those in the thick pipe, and the distribution of the principal directions is also similar to that in the thick wall pipe (refer to Section 4.3.2 and see Figure 4.7).

As for the normalized most compressive principal stresses in the thin wall pipe under edge loading, the distribution patterns in all three cases are very similar to those in the thick wall pipe, and the peak magnitudes are slightly higher than those in the thick wall pipe (refer to Section 4.3.2 and see Figure 4.8).

4.5 CONCLUSION

So far, analyses of six types of loads (three 'edge' loads and three 'diagonal' loads) and two pipe sizes (the thick wall and the thin wall pipe) have been described in this chapter. The localization of the applied load induces not only high concentrated compressive stresses but also high tensile stresses in the concrete pipe. The stresses in all load cases are neither uniformly distributed across the thickness of the pipe nor linearly distributed in the circumferential direction, but are more complex three-dimensional patterns. High stresses appear in two regions at the pipe joints near the two loaded corners. In general, the more

localised the applied load, the higher the maximum tensile stress. Moreover, under a similar load intensity, the load distribution in the cases E2 and D2 produces higher tensile stresses at the pipe joints than in the case E3 and D3.

From the numerical results of the numerical model A in this chapter, some conclusions are drawn as following:

(1) The greatest potential damage is at the pipe joint, that is, cracking due to the high tensile stresses or crushing due to the very high compressive stresses. Due to the very low tensile strength in the concrete pipe, another possible type of damage is cracking at the middle length of the pipe on the internal surface under the 'edge' loading condition and in the region of $\theta = 90^0$ on the external surface under the 'diagonal' loading condition. For the cases studied, the joint behaviour is most severe. However, the loading conditions in this chapter are extremely severe ones due to high pipeline misalignment and uneven pipe end; presumably, loading on a larger end area would result in reduction in stresses at the pipe joint.

(2) Stresses in the thin wall pipe exceed those in the thick wall pipe by more than the thickness ratio. This means that the pipe capacity is not proportional to the pipe thickness. Presumably this is a result of local bending effects in the pipe wall (under the same bending moment in the pipe wall, the maximum stress in the pipe is proportional to $\frac{1}{(pipe\ thickness)^2}$).

(3) Diagonal loading is more severe. However, this may be because of the effect of local constraints which might deviate from the boundary conditions in practice as discussed in Section 4.3.2.

(4) Local joint stresses are greatly influenced by the distribution of the joint loads and the stresses change dramatically across the pipe thickness at the joint. This suggests that careful joint design is needed.

(5) To obtain better understanding about the pipe behaviour, a few more aspects should be examined, for example the interaction between the pipe and its surrounding soil and the interaction between the adjacent pipes.

4.6 BACK ANALYSIS OF RIPLEY'S EXPERIMENT

To model the effect of the misalignment of the pipe line in practice, Ripley(1989) carried out some laboratory tests. Two sizes of pipe, the thick wall and the thin wall pipe, were used in his tests and the dimensions of the test pipes are the same as those shown in Figure 4.1. A misalignment apparatus shown in Figure 4.11 was designed by Ripley in his tests to model the extreme loading condition with a limited area of contact. The yokes in the apparatus could be arranged to provide support to the pipe and could be adjusted at different angles to simulate different misalignment conditions, that is, the 'edge' and the 'diagonal' loading condition as shown in Figure 4.12(a) and 4.12(b). During the tests, the strains at the middle length section (z = 116mm) of the concrete pipe were measured with strain gauges; the load distributions on the pipe ends were not measured.

The purpose of the back analysis is to compare the numerical results with the measured strains and to check the effectiveness of numerical model A. The pipe is assumed to be linearly elastic with the Young's modulus E_c = 31700MPa and the Poisson's ratio μ_c = 0.2 as found by Ripley in his laboratory tests. In the numerical back analysis, the finite element mesh is the same as that used in Section 4.3 shown in Figure 4.1 since the loads are again symmetrical about the plane of $y = 0$. Due to the deformation of the yokes, the loading areas are not extremely small, but could be up to one third of the cross section of the pipe as found by Ripley (1989) and the contact areas between the pipe and yokes are also fairly large. Since there is no measured information about the load distribution on the pipe ends, a linear distribution of the applied load is assumed over one third of the cross section of the pipe as shown in Figure 4.13(a) and 4.13(b) for the 'edge' and the 'diagonal' test. The total applied load in the analysis is P = 5kN (on half of the pipe) to simulate an early stage in the test since an elastic pipe model is used in the analysis. There is also no measured information on the contact area between the concrete pipe and the yokes, and the contact area is assumed over about 70 degrees along circumferential direction (35 degrees for half of the pipe in the

analysis) and the nodes within this area are fixed in the x direction to model the support of the yokes as shown in Figure 4.13(c) and 4.14(d). The boundary conditions also include the symmetrical condition on the plane $y = 0$.

The strains measured during the test were all on the external and the internal surface of the pipe in a two-dimensional state, this is, ε_θ, ε_z and $\gamma_{\theta z}$. In the numerical analysis, the strains are calculated at Gauss points, that is, the numerical strains on a surface of r = constant very near the external or the internal surface are used in the comparison. The numerical strains chosen for comparison are in the same two-dimensional state as the measured ones. For the convenience of comparison, several tests from Ripley's experimental data (1989) are chosen to represent different situations. Under 'diagonal' loading, test 8 is chosen for thick wall pipe and test 16 for thin wall pipe; and under 'edge' loading, test 19 is chosen for thick wall pipe and test 23 for thin wall pipe. The tests chosen in comparison are typical from the point of view of average measured strains.

The most tensile (1st) principal microstrain and the most compressive (2nd) principal microstrain under the 'diagonal' loading condition in the thick wall pipe and in the thin wall pipe are shown in Figure 4.14(a) and 4.14(b) respectively. In the figure, the squares and the crosses denote the most tensile principal microstrains on the external surface of the pipe from numerical analysis and from experiment, and the triangles and the circles denote the most compressive principal microstrains on the external surface of the pipe from numerical analysis and from experiment respectively. From the figure, it is very clear that the numerical results and the experimental data agree well.

The most compressive principal microstrains under the 'edge' loading condition in the thick wall pipe and in the thin wall pipe are shown in Figure 4.15(a) and 4.15(b) respectively.

In the figure, the squares and the crosses denote the principal microstrains on the external surface of the pipe from numerical analysis and from experiment, and the triangles and the circles denote the principal microstrains on the internal surface of the pipe from numerical analysis and from experiment respectively. Again, the numerical results and the experimental data agree well except for the strain at point G (r = 100mm and $\theta = 180^0$). In theory, the compressive strain at the point G on the external surface should be higher than that at the point H on the internal surface under the 'edge' loading condition as indicated by the numerical results. The experimental data show that the compressive strain at point G is just over half of that at point H. This experimental result is very difficult to explain in theory and further investigation may be needed.

The results above suggest that numerical mode A is reliable to model the tests in the early stage in which the pipe is behaving in a linearly elastic manner. To obtain more detailed information about the behaviour of the concrete pipe at late test stage with cracks, a complex concrete material model is needed in future.

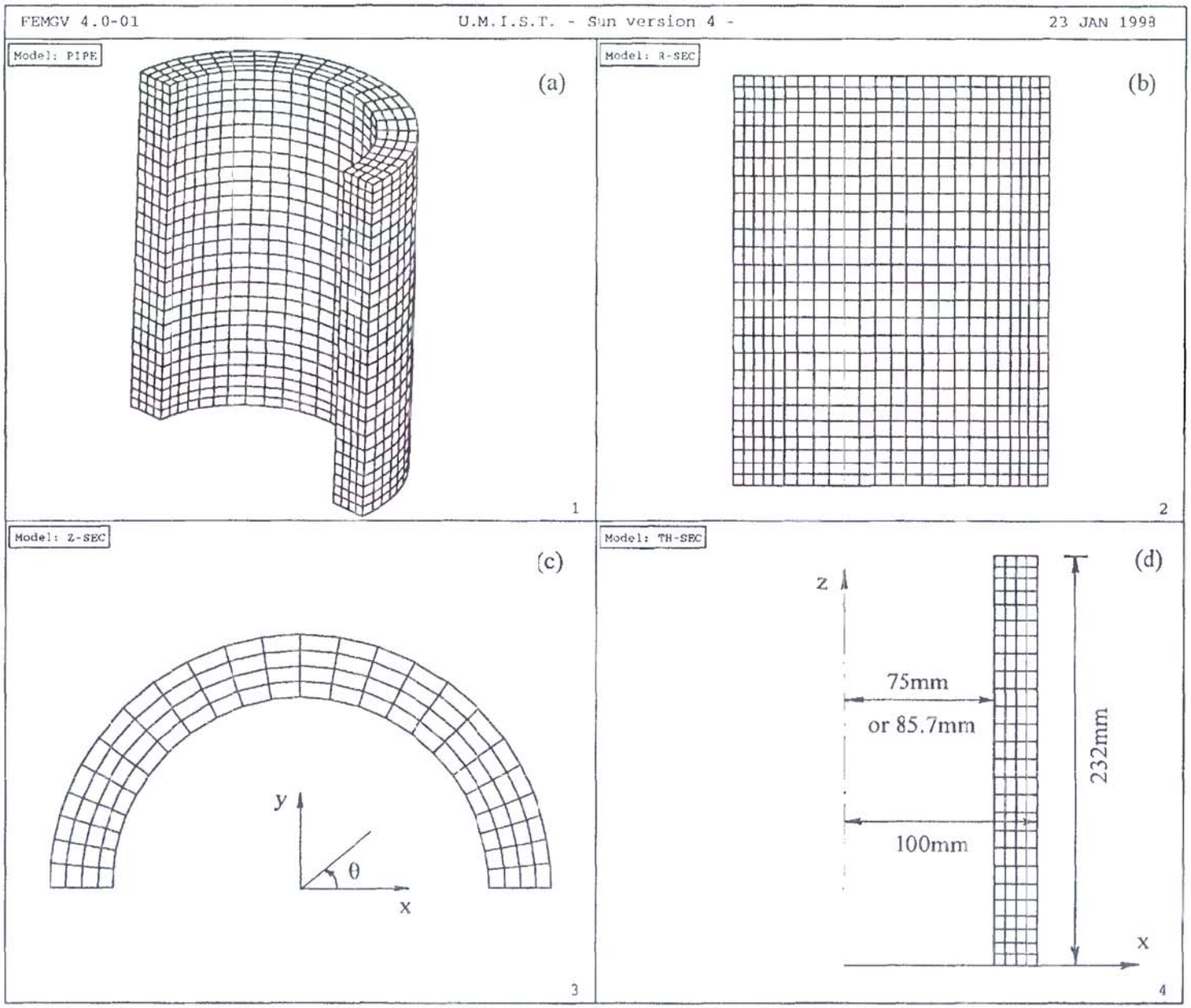

Figure 4.1 Numerical model A and its FE mesh

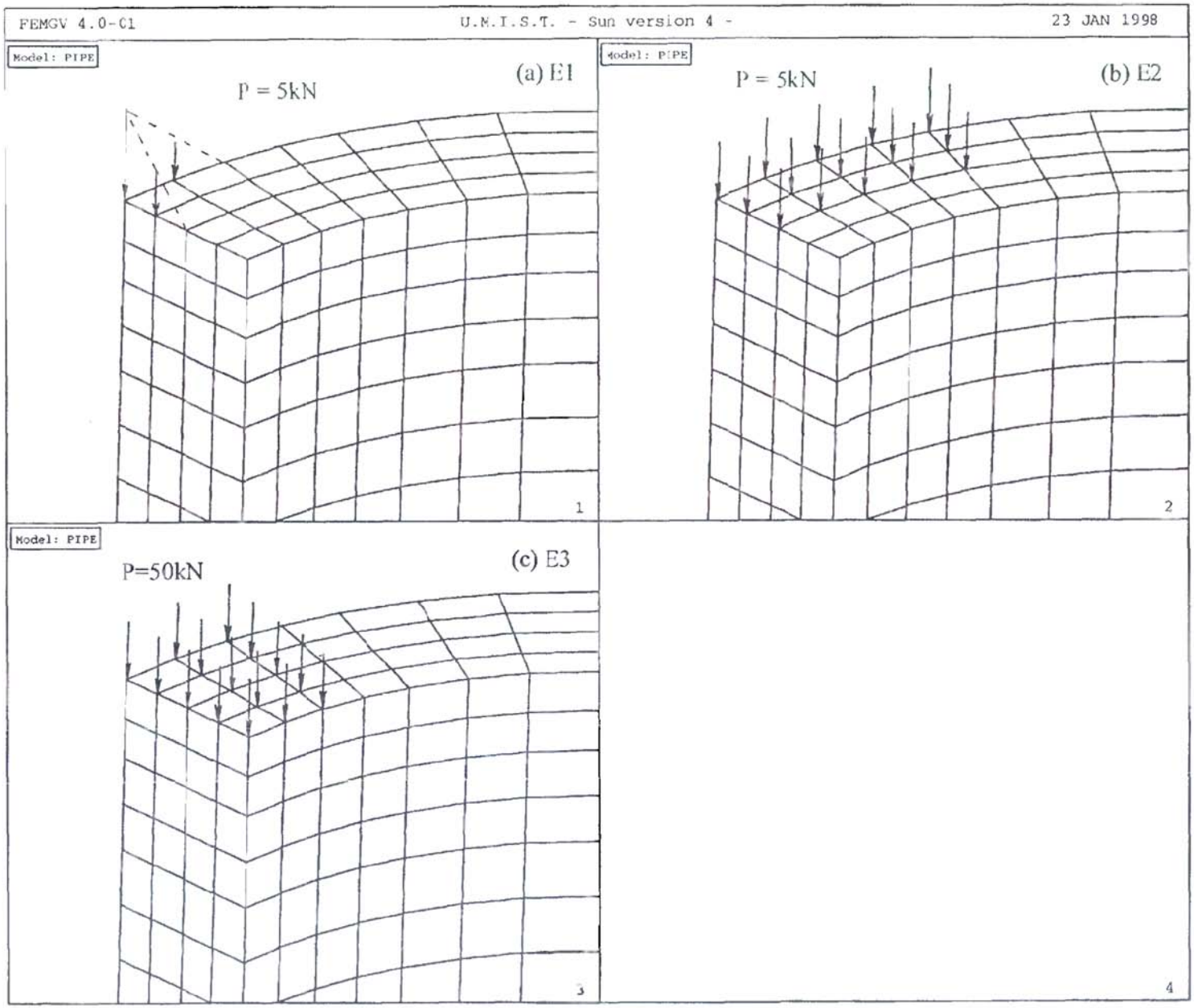

Figure 4.2 Three load distributions on the upper pipe end

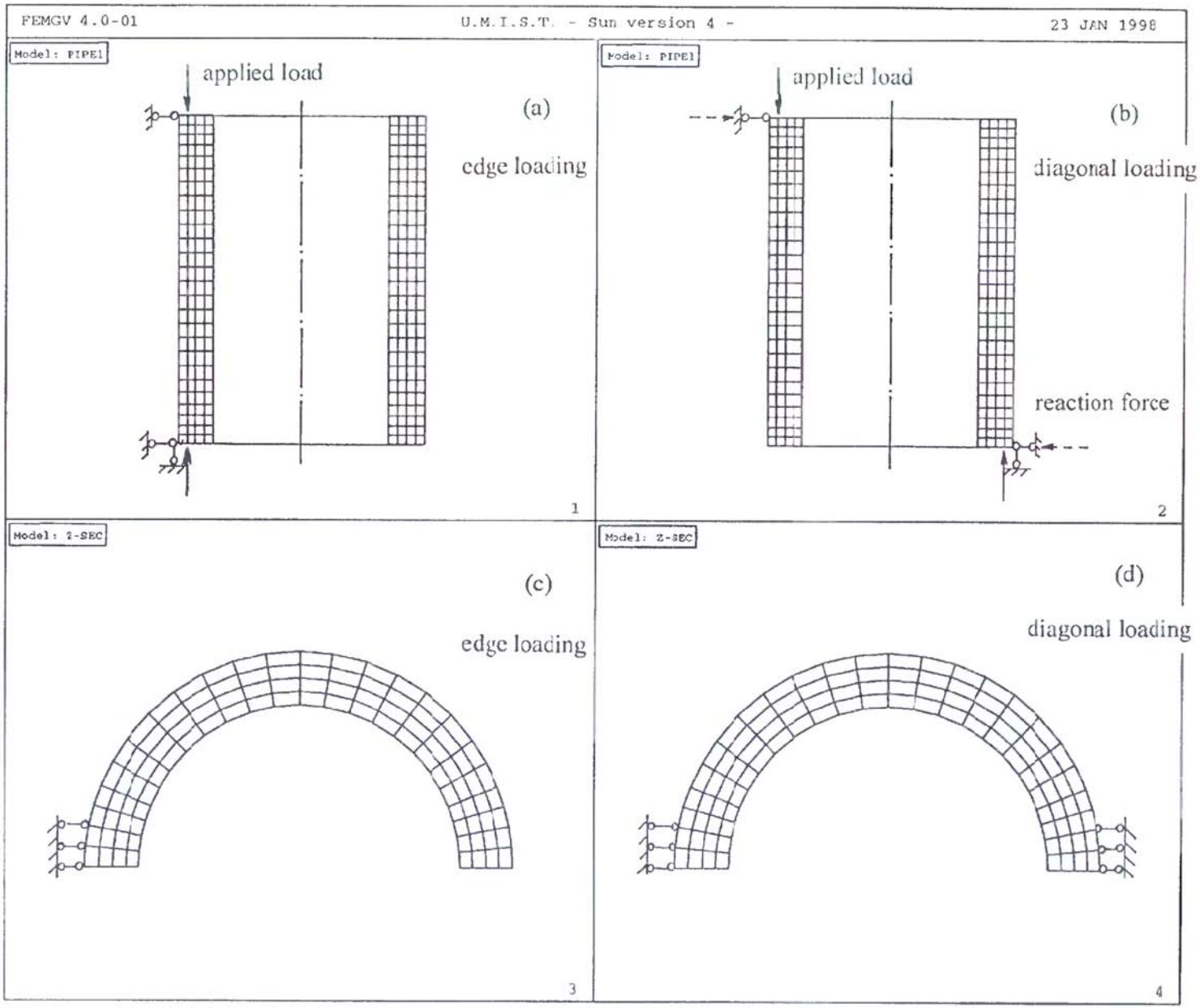

Figure 4.3 Boundary condition under 'edge' and 'diagonal' loading

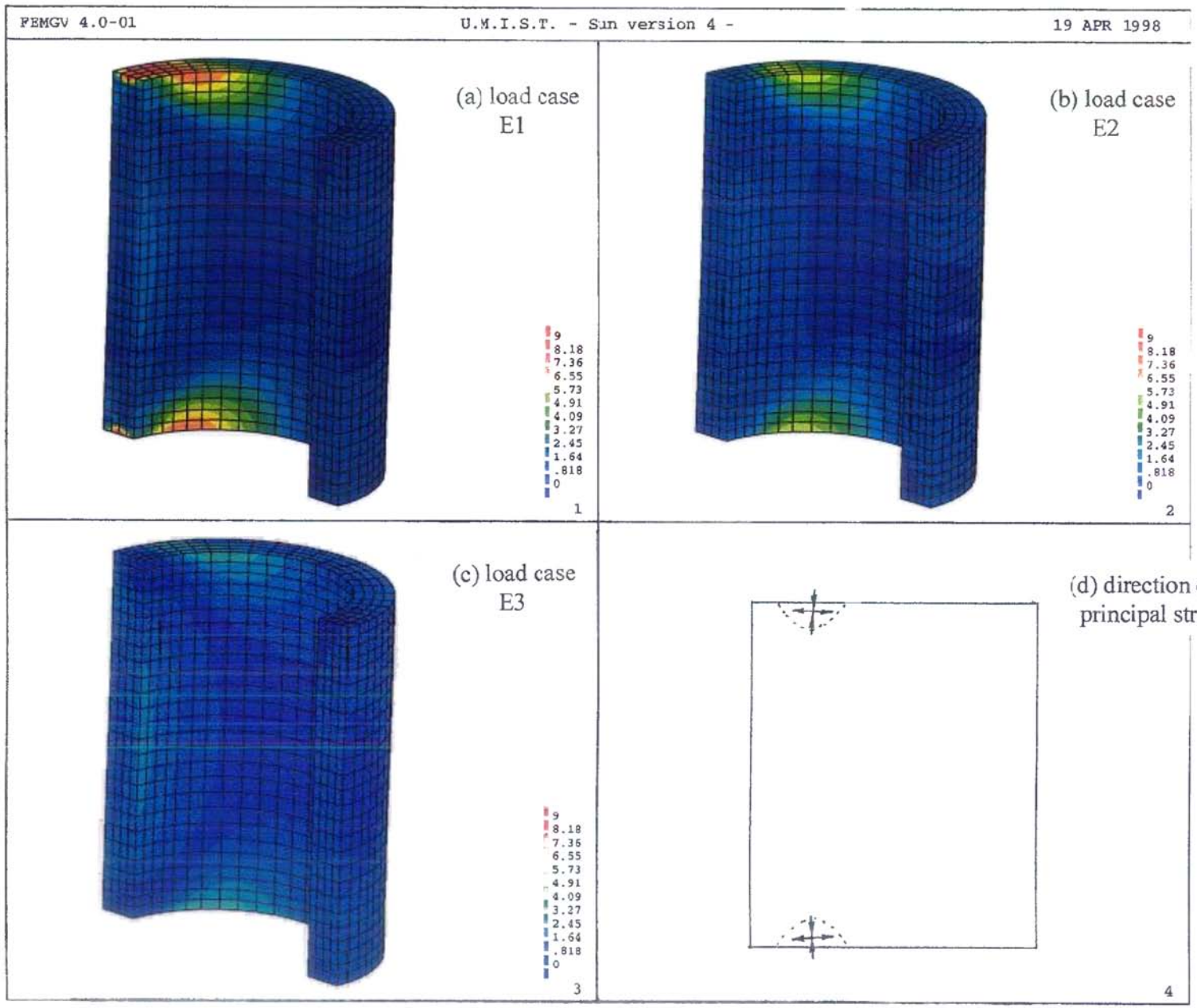

Figure 4.4 Normalized most tensile principal stresses in the thick wall pipe under 'edge' loading

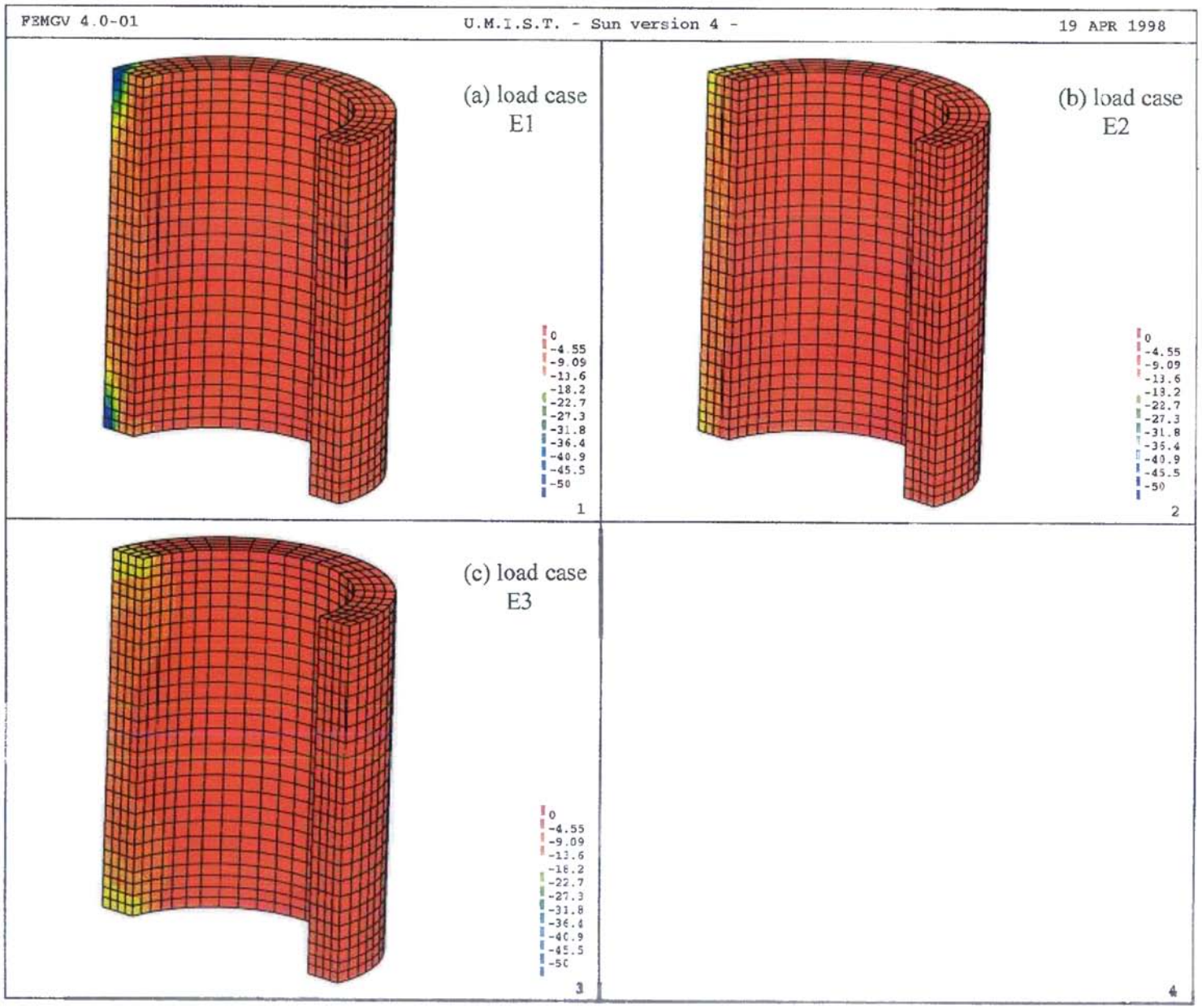

Figure 4.5 Normalized most compressive principal stresses in the thick wall pipe under 'edge' loading

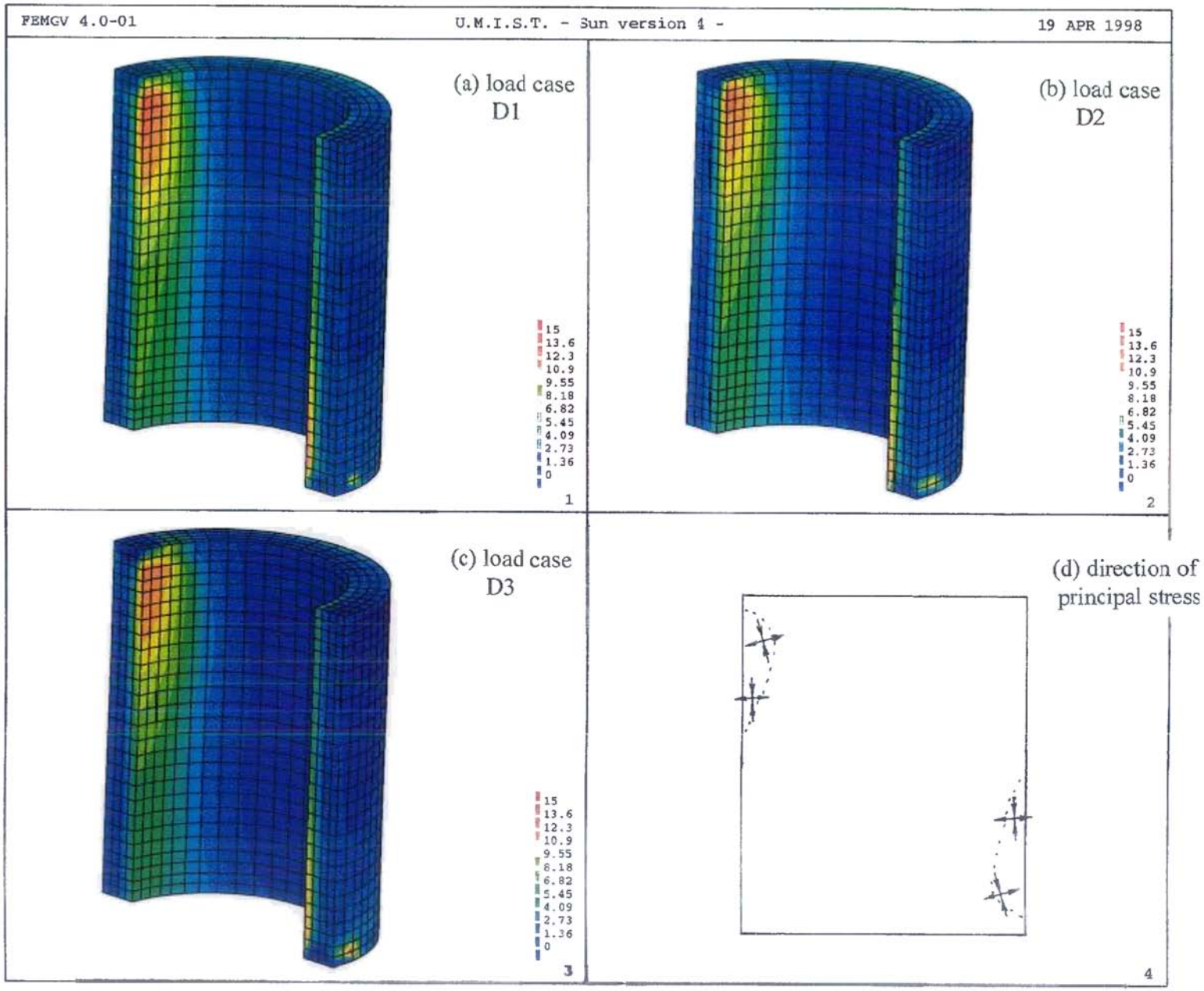

Figure 4.6 Normalized most tensile principal stresses in the thick wall pipe under 'diagonal' loading

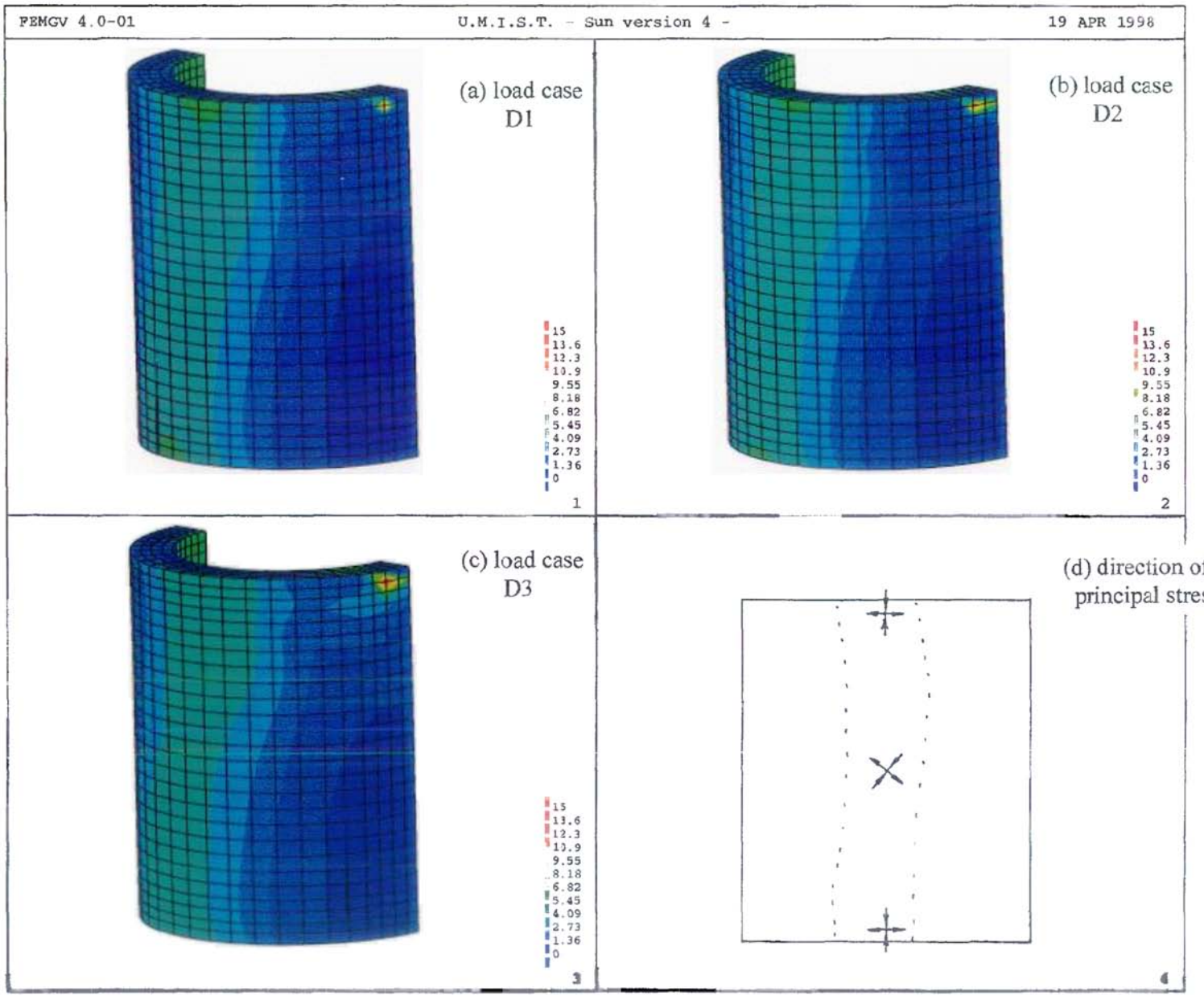

Figure 4.7 Normalized most tensile principal stresses in the thick wall pipe viewed from opposite direction under 'diagonal' loading

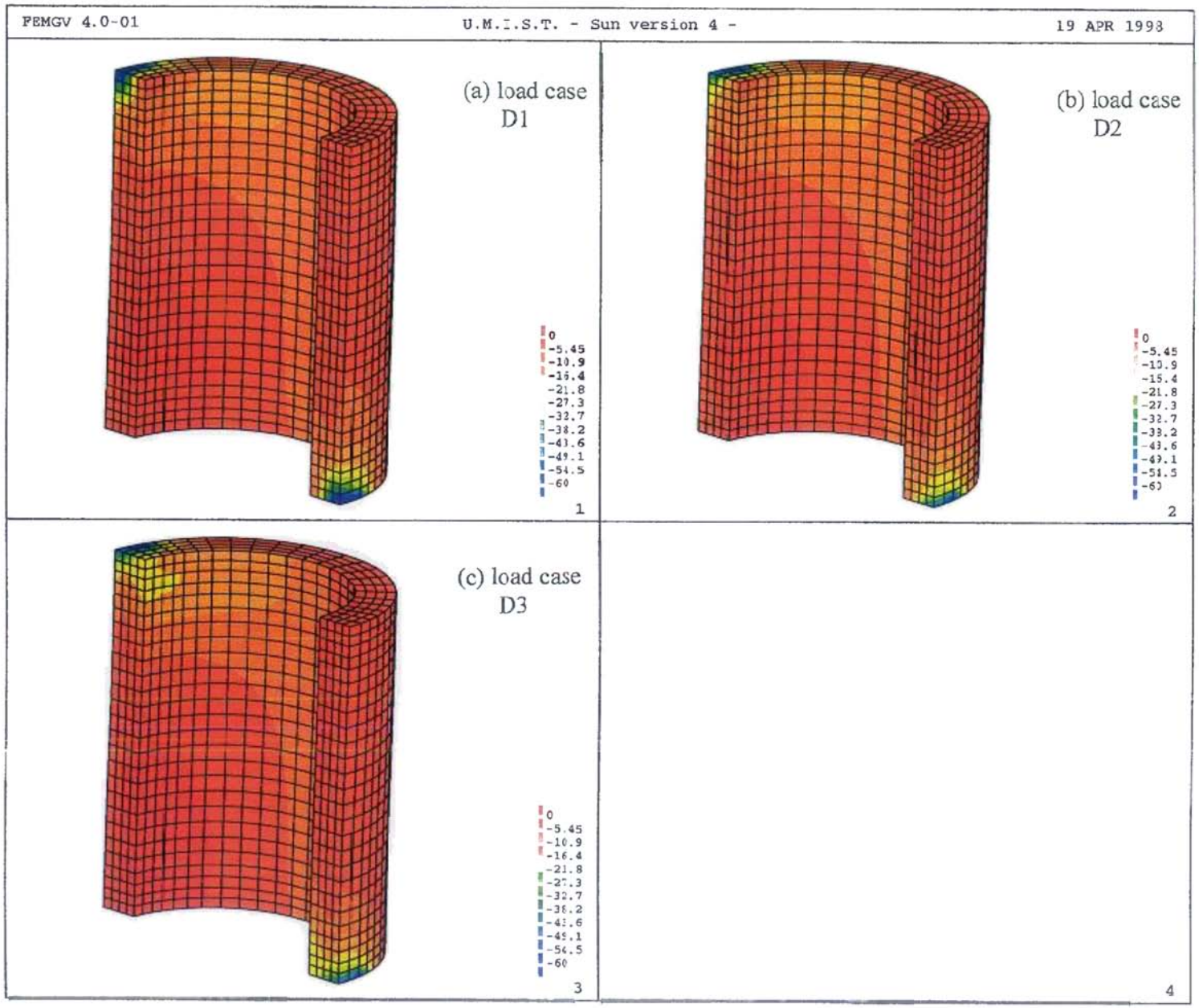

Figure 4.8 Normalized most compressive principal stresses in the thick wall pipe under 'diagonal' loading

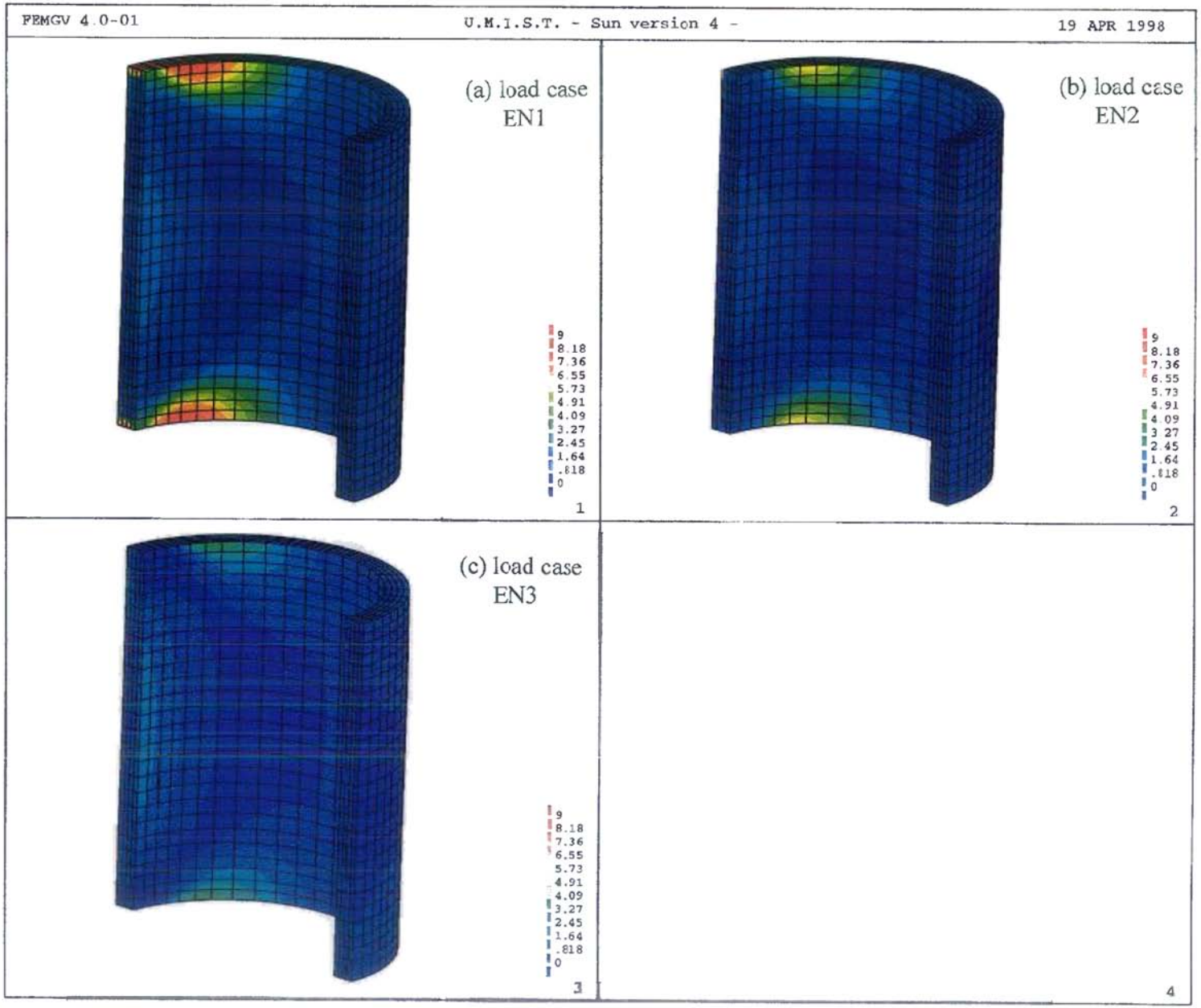

Figure 4.9 Normalized most tensile principal stresses in the thin wall pipe under 'edge' loading

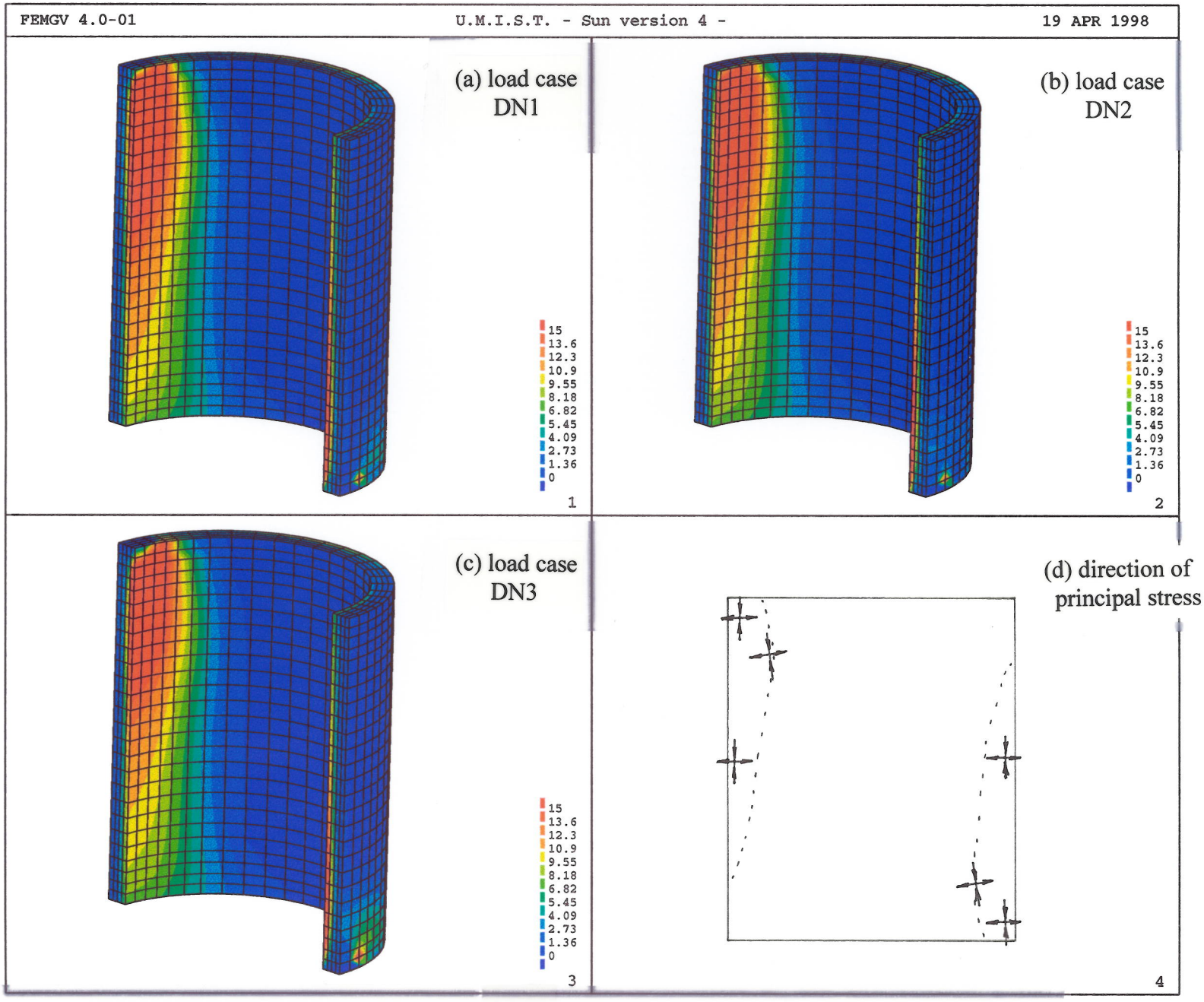

Figure 4.10 Normalized most tensile principal stresses in the thin wall pipe under 'diagonal' loading

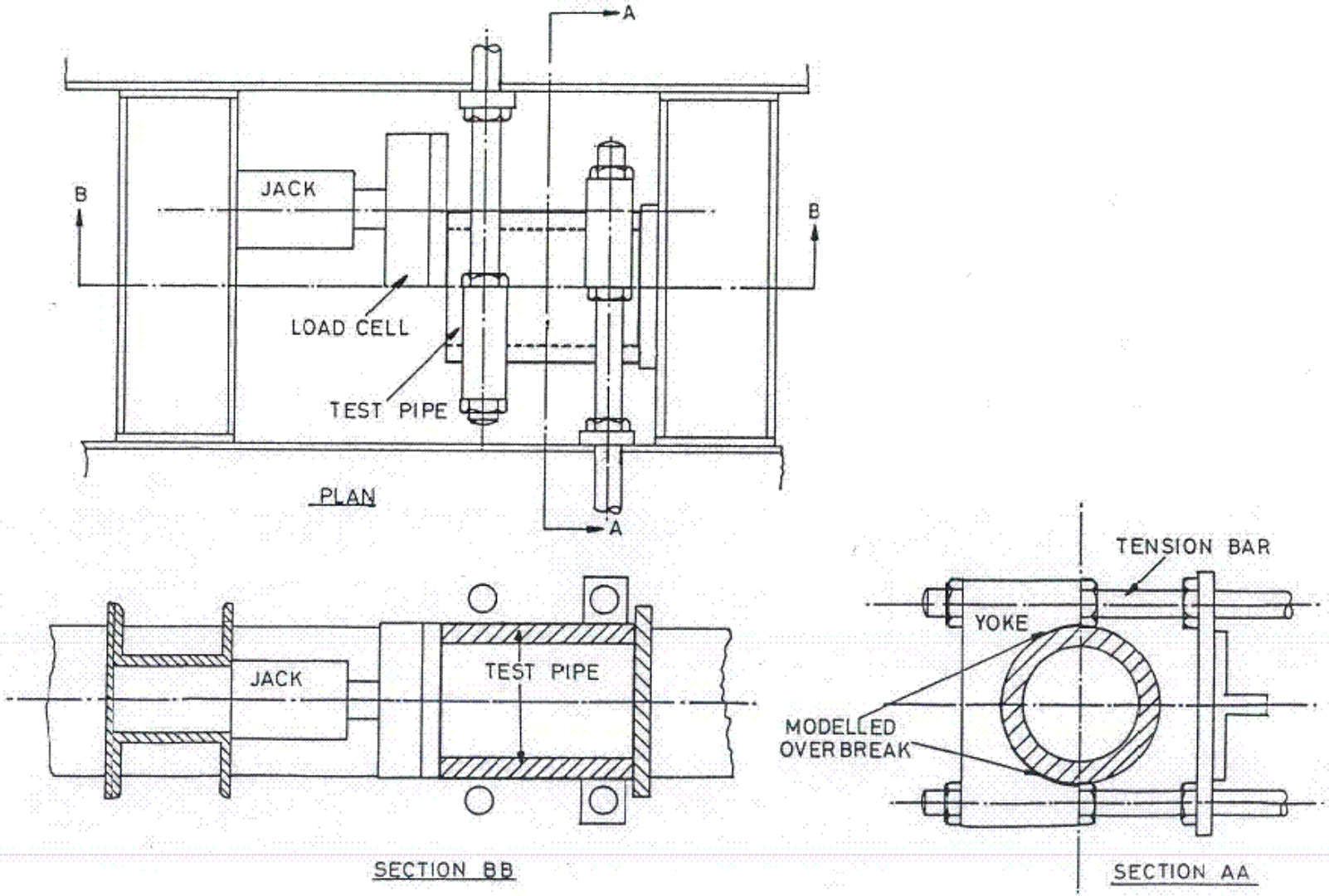

Figure 4.11 Misalignment apparatus general arrangement (from Ripley 1989)

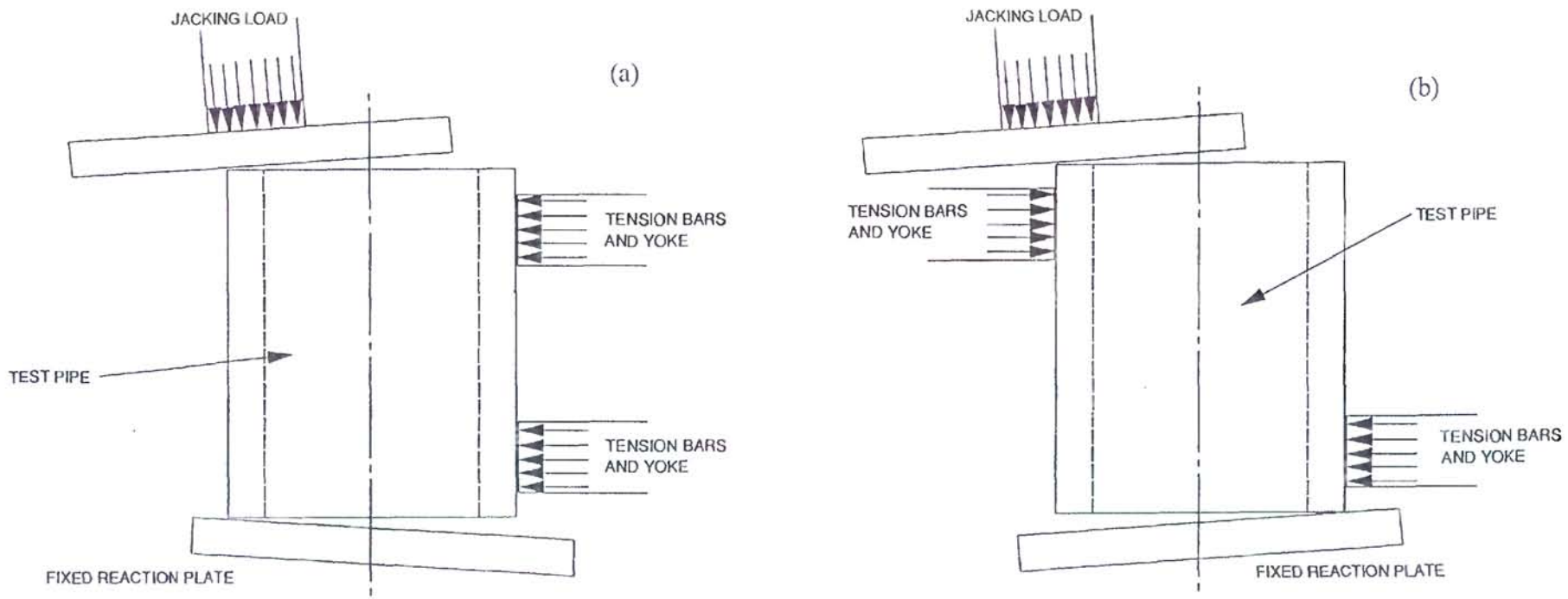

Figure 4.12 Loading arrangement for both edge and diagonal test (from Ripley 1989)

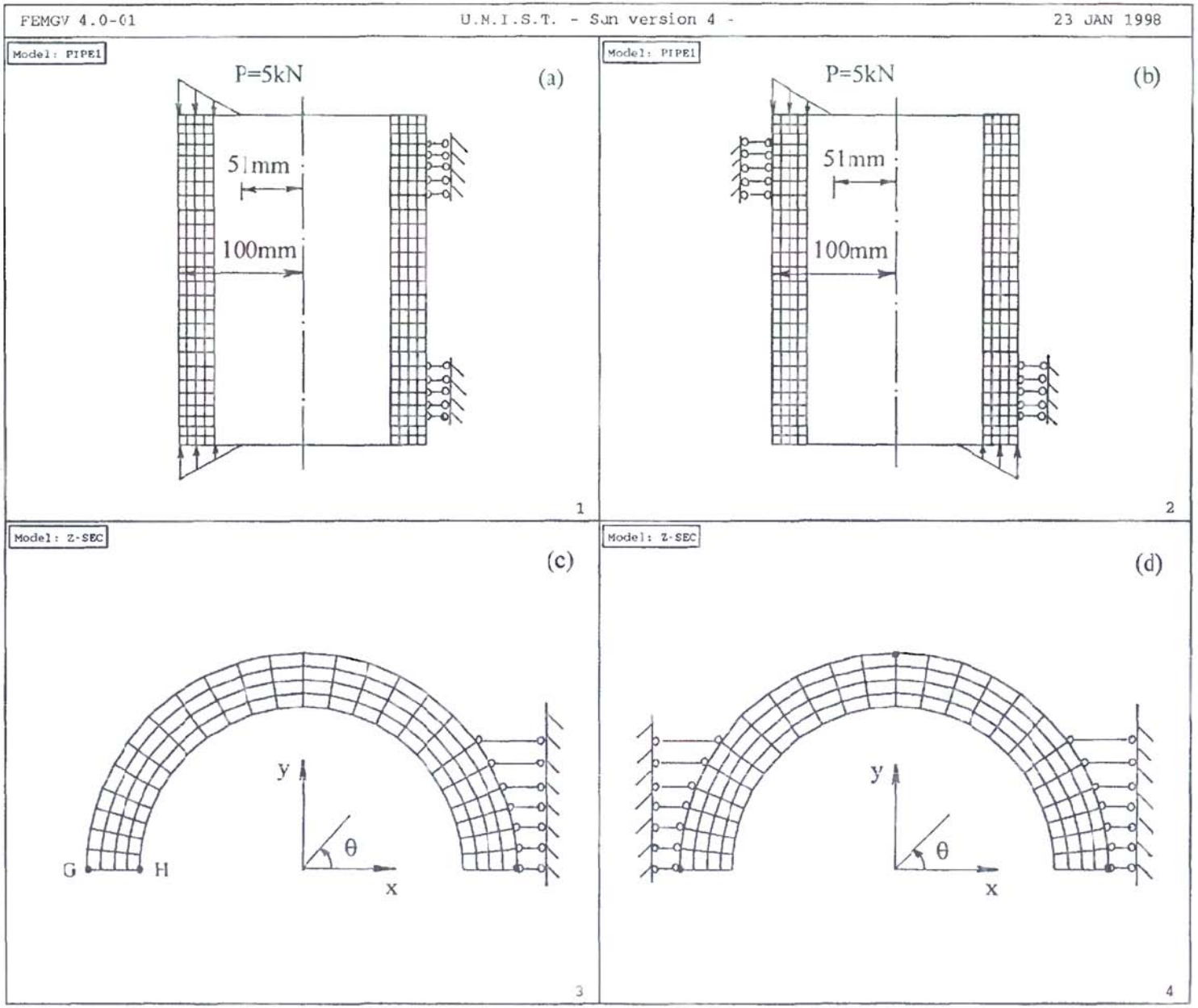

Figure 4.13 Loading and boundary condition of Numerical model A for back analysis

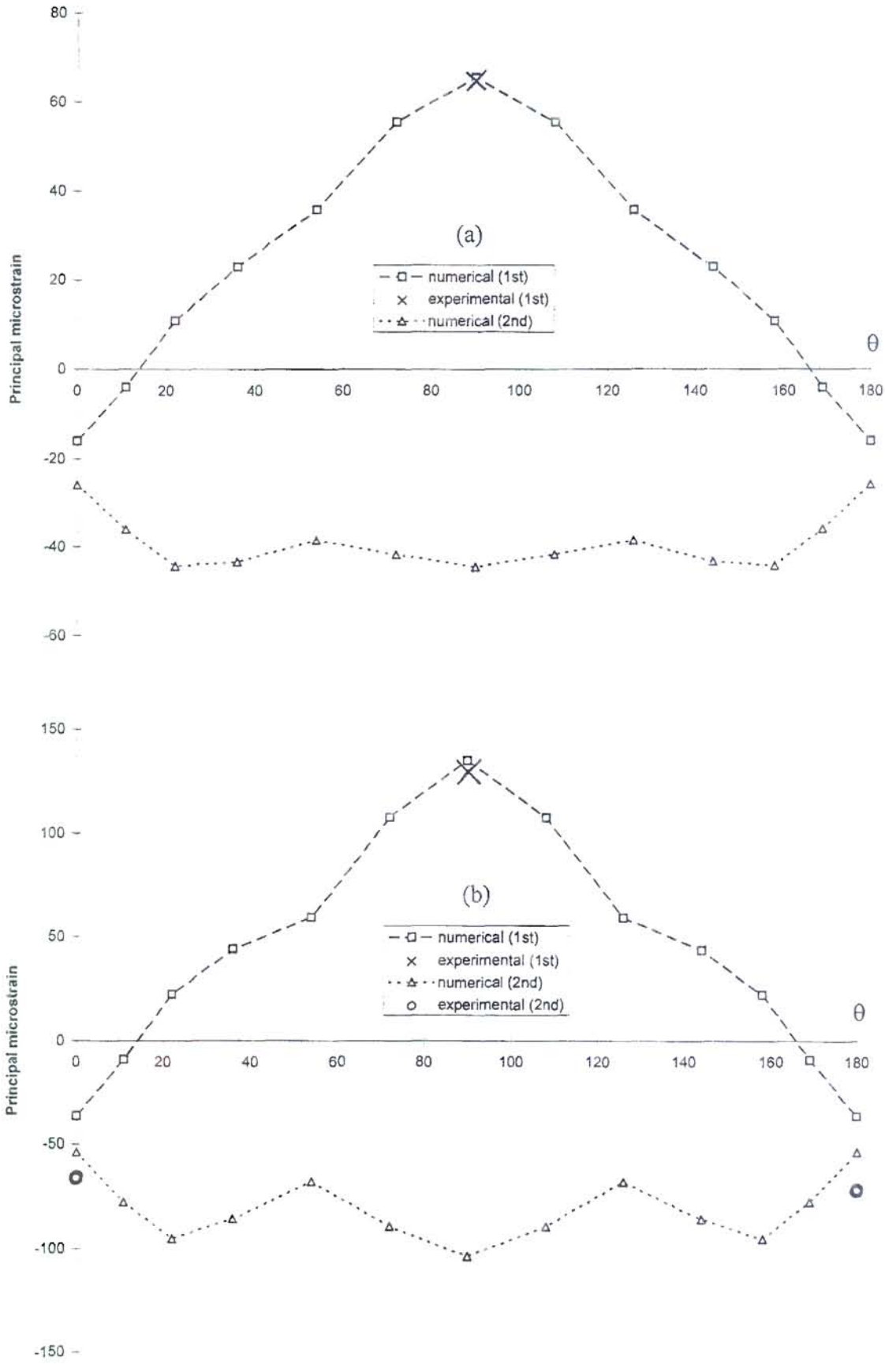

Figure 4.14 Comparison between numerical results and experimental data under 'diagonal' loading

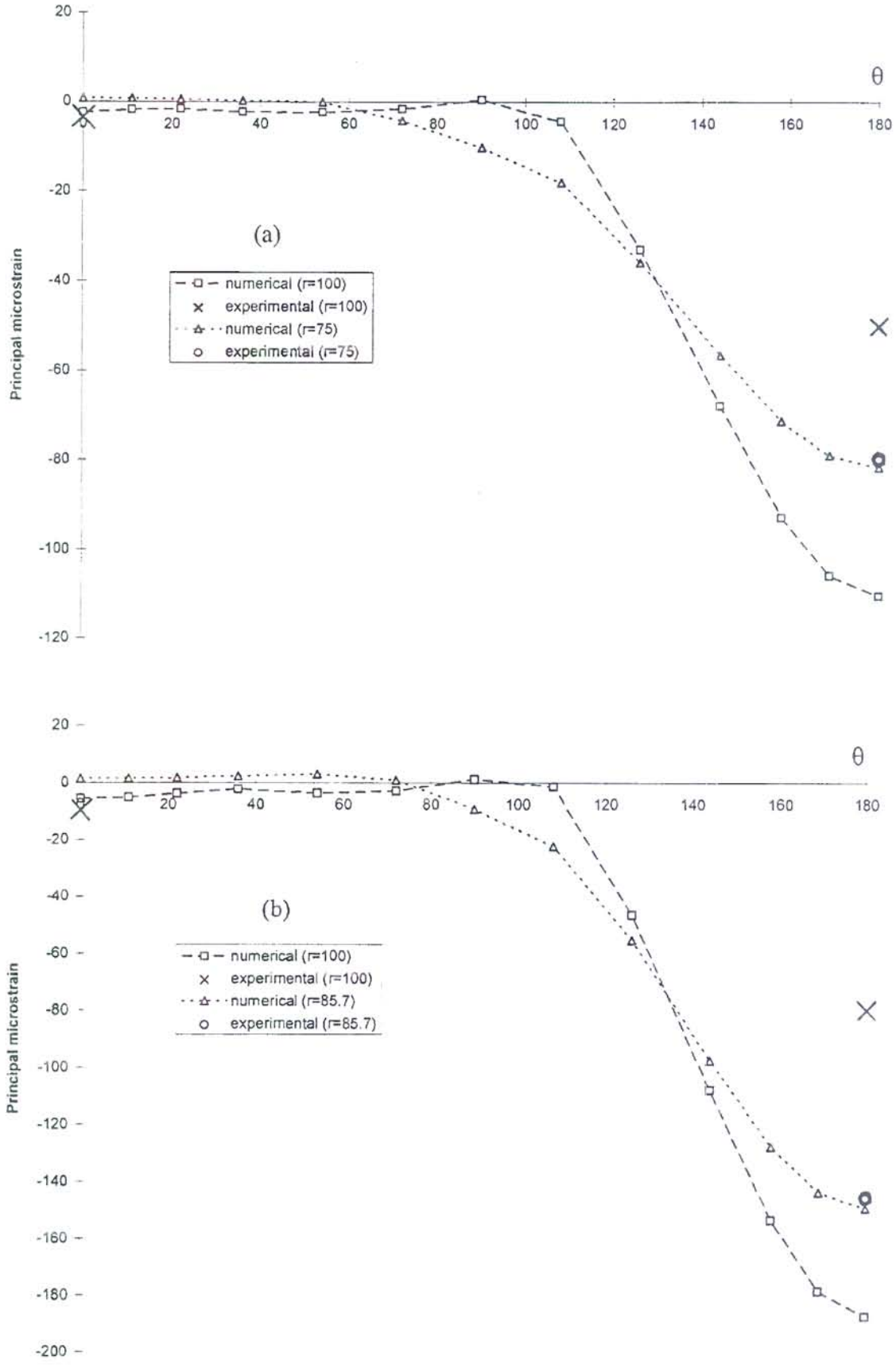

Figure 4.15 Comparison between numerical results and experimental data under 'edge' loading